ANNUAL REVIEWS

Annual Review of Physical Chemistry

Enhancing Analytical Separations Using Super-Resolution Microscopy

Nicholas A. Moringo,[1] Hao Shen,[1] Logan D.C. Bishop,[1] Wenxiao Wang,[2] and Christy F. Landes[1,2,3]

[1]Department of Chemistry, Rice University, Houston, Texas 77251, USA; email: cflandes@rice.edu

[2]Department of Electrical and Computer Engineering, Rice University, Houston, Texas 77251, USA

[3]Smalley-Curl Institute, Rice University, Houston, Texas 77251, USA

Annu. Rev. Phys. Chem. 2018. 69:353–75

First published as a Review in Advance on February 28, 2018

The *Annual Review of Physical Chemistry* is online at physchem.annualreviews.org

https://doi.org/10.1146/annurev-physchem-052516-045018

Keywords

industrial drug purification, chromatography, single-molecule spectroscopy

Abstract

Super-resolution microscopy is becoming an invaluable tool to investigate structure and dynamics driving protein interactions at interfaces. In this review, we highlight the applications of super-resolution microscopy for quantifying the physics and chemistry that occur between target proteins and stationary-phase supports during chromatographic separations. Our discussion concentrates on the newfound ability of super-resolved single-protein spectroscopy to inform theoretical parameters via quantification of adsorption-desorption dynamics, protein unfolding, and nanoconfined transport.

1. INTRODUCTION

As of 2015, introducing a biological pharmaceutical, known as a biologic, to market cost ~$2.6 billion (1), of which ~50% can be attributed to separation and purification (2–4). The most common separation method, chromatography, is used everywhere from laboratory-scale refinement to downstream industrial purification (5–7). With worldwide medical use of biologics only increasing (8–10), it is time to address the mismatch between the status quo of empirical separations and the strong need for predictive separations at both bench and industrial scales. The lack of predictive chromatography can be attributed both to the complexity of the underlying physics and chemistry, which hampers computation, and to gaps in experimental analyses, with ensemble assays such as adsorption isotherms masking underlying heterogeneity.

The effort to model and thereby improve separations began as early as the 1920s (11, 12). To date, however, there is still no comprehensive theory that links the multiscalar dynamic processes occurring in a chromatographic column to observable elution profiles. Instead, users at laboratory and industrial scales are left to rely on empirical equations (13) that suffer from oversimplification. More elegant theoretical advances made as early as the 1950s (14) were not adapted for the simple reason that there was no experimental way to link the underlying physics to a quantifiable observable. The advent of single-molecule methods in general, and super-resolution methods in particular, makes it possible to extract the theoretical parameters driving chromatographic separations.

Super-resolution microscopy (15) is a noninvasive tool that quantifies many of the multifaceted components present in protein separations (16), allowing for single fluorescently labeled analytes such as biologic molecules to be monitored in situ in real time. For example, super-resolution techniques can provide high spatial and temporal resolution of individual molecules undergoing transport dynamics in a high-throughput fashion (17–20). Access to such detail is often challenging with traditional techniques (21) but is readily achieved with super-resolution microscopy. Additionally, super-resolution techniques monitor molecules exploring heterogeneous local environments. Super-resolution microscopy is a robust field enjoying rapid improvements in spatial and temporal resolution and in the types of samples that can be studied (15, 22), providing an experimental framework as well as motivating theoretical developments.

In this review, we summarize super-resolution results from our research group and others focused on advancing our understanding of the fundamental physical chemistry driving protein separations. We first cover the evolution of chromatographic theory and the assumptions made in each model, with an emphasis on the origins of elution profile broadening (23). Next, we highlight the utility of single-molecule techniques to uncover three main dynamic processes that occur in protein separation systems: adsorption-desorption processes at the stationary phase, protein unfolding and competition on support materials, and diffusion within porous column media. Last, we discuss the future outlook and directions for achieving a comprehensive and predictive chromatography model based on new insights provided by super-resolution microscopy.

2. THEORY AND GUIDING ASSUMPTIONS

The primary concern of chromatographic theory is providing a mathematical framework to quantify the structure of an elution profile and define the quality of a chromatographic separation. An elution profile should approach a Gaussian lineshape, an eventuality described by the central limit theorem (24, 25). This is realistically unobtainable, since the central limit theorem assumes that the collection of observations all originate from the same parent distribution (26). Complex interactions between the analyte and stationary phase cause transport anomalies that create a variety of elution distributions, made evident by both broadening and skewing of the elution profile (**Figure 1**). Elution asymmetries such as skewing decrease the separation fidelity and decrease

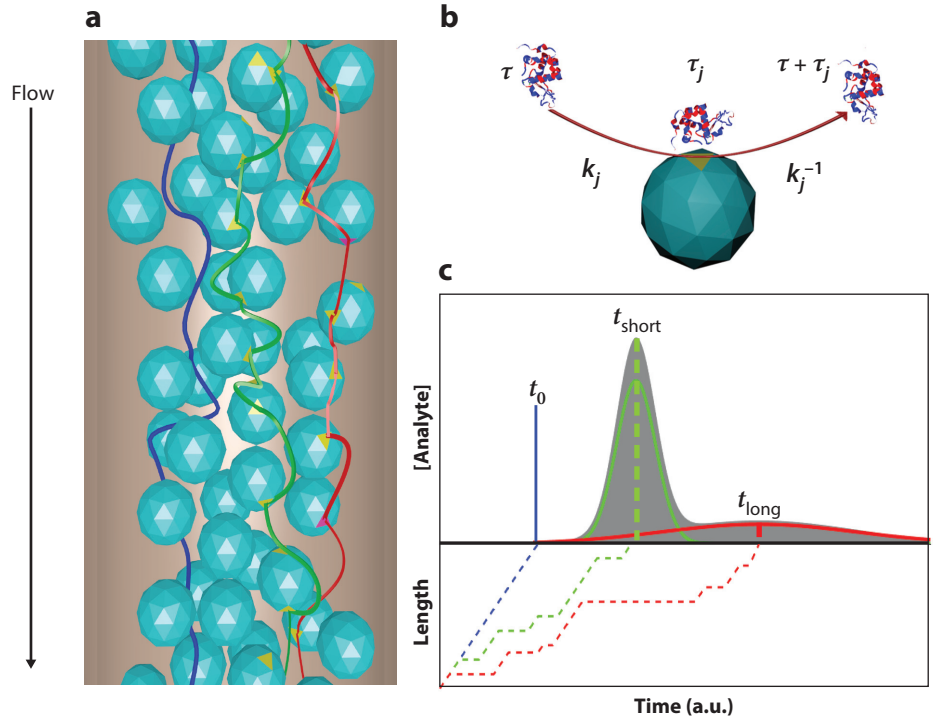

Figure 1

The Giddings–Eyring model constructs an elution curve from the sum of several thousand molecular trajectories with variable histories of adsorption. (*a*) A schematic depiction of a chromatographic separation, where the stationary phase is represented as cyan beads and adsorption events as discoloration on the bead surface (*yellow* = short-lived adsorption; *pink* = long-lived adsorption). The three possible adsorption histories for a molecule moving through a column are represented by colored trajectories: no adsorption events (*blue*), homogeneous adsorption events (*green*), or a mixture of different adsorption events (*red*). (*b*) Depiction of α-lactalbumin [Protein Data Bank: 1A4V (29)] adsorption event at bead support with adsorption rate (k_j) and residence time (τ_j) dictated by desorption rate (k_j^{-1}). The total retention time (t_s) is the sum of these adsorption events with the constant amount of time spent in the mobile phase, t_0. (*c*) The summation of many of these molecular random walks (*bottom*) leads to the formation of an elution curve (*top*). Molecules experiencing no adsorptions elute simultaneously, under the assumption of uniform flow speed, forming a Dirac delta at t_0 (*blue*). Molecules undergoing a series of adsorption events originating from the same distribution converge to a Gaussian lineshape (*green*) about the average retention time t_{short}. Molecules experiencing infrequent, long-lived adsorption events then form a tail to the distribution (*red*) about t_{long}.

product yield. The goal in physically describing a chromatographic process, then, is to identify the root causes of these asymmetries, making it possible to remove them by predictive methods rather than by empirical optimization.

Three main branches of theory used to explain the shape of an elution profile were posited in the 1940s and 50s. Chronologically, these are the plate model (27), differential mass balance equations (28), and the stochastic processes model (14). These models differ primarily in their treatment of the chromatographic system. The plate model and differential mass balance methods assume a macroscopic view and attempt to track elution progress through creation of a detailed mass balance differential. In contrast, theories based on the stochastic processes model treat the elution profile as a statistical entity constructed from several thousand independent analyte trajectories

(**Figure 1*a***), detailing the adsorption events (**Figure 1*b***) undergone by an analyte as it traverses down a column. Modeling the elution profile as the sum of thousands of molecular histories (**Figure 1*c***) establishes a connection between the underlying dynamics occurring between analyte and stationary phase and the macroscale observable.

All of these theories operate on various assumptions that oversimplify the chromatographic process to make the mathematics used to create an elution profile tractable. For example, there is the assumption that molecules do not diffuse in the axial direction and that the adsorption isotherm is linear in the regime of interest (14, 28). Linearity of the isotherm implies that the analyte is sufficiently dilute for there to be no competition for sites on the stationary phase, which allows the complete elution profile to be treated as the sum of the distributions of each type of site. The range of difficulties introduced by assuming isotherm linearity includes the need to treat the binding probability of the analyte as unrelated to its position in the column. However, the shifting probability of adsorption created by stationary-phase heterogeneity can be approximated with an average adsorption constant k with the assumption that an analyte molecule fluctuates through the full range of probabilistic densities a sufficient number of times (14).

2.1. Plate Model

The plate model for separations was created as an analog to the description of distillation by Martin & Synge (27), viewing the separation process as a series of equilibrium states between plates. Separatory efficacy is often described as the height equivalent to a theoretical plate (HETP), originally described by Peters (12). Elution is then the motion of analyte mass between neighboring plates. The mass balance differential that describes this motion through the column assumes a set transfer of mass through the volume of both stationary and mobile phases in a plate. Balancing the influx and outflux of mass can be modeled using a differential equation (30):

$$V_{\mathrm{m}}\frac{\mathrm{d}c_r}{\mathrm{d}t} + V_{\mathrm{s}}\frac{\mathrm{d}q_r}{\mathrm{d}t} = \mu\,(c_{r-1} - c_r)\,, \qquad 1.$$

where μ is the mobile phase flow velocity, r is the plate number, and $V_{\mathrm{m}}/V_{\mathrm{s}}$ represent the total volume and c_r/q_r the analyte concentrations in the mobile/stationary phases, respectively. Assuming that the transitions of analyte molecules from plate to plate follow a Poisson distribution, the final probability density function becomes (31):

$$f(t) = \frac{\sqrt{N}}{\sqrt{2\pi t_{\mathrm{r}}}}\exp\left[-\frac{N}{2}\left(\frac{t}{t_{\mathrm{r}}} - 1\right)^2\right]. \qquad 2.$$

Here, N is equivalent to the number of plates and t_{r} is the retention time. Should N be sufficiently large, as it traditionally is for chromatographic separations, the probability density function converges to the Gaussian shape.

2.2. Differential Mass Balance

Lapidus & Amundson (28) introduced a more complex mass balance equation that incorporates terms for the diffusion coefficient (D) and examines the change of concentration across a slice of the column (z) as well as the porosity of the stationary phase (α). The resulting complete differential presents a major theoretical challenge, as its solvability is dependent on the boundary conditions chosen (28):

$$\frac{\delta c}{\delta t} + \alpha\frac{\delta q}{\delta t} + \mu\frac{\delta c}{\delta z} = D\frac{\delta^2 c}{\delta z^2}\,. \qquad 3.$$

The original solution for an infinite column with an infinitely narrow injection peak was later expanded with other boundary conditions by Guiochon et al. (32). Noting that the elution profile goes to zero as it moves further from the average retention time, manipulation of this differential leads to an elution profile equivalent to Equation 2.

Differential mass balance became the center of theoretical interest, as it offered direct comparisons to the classic HETP metric and offered more accurate results than alternatives (12). The full differential (Equation 3), commonly derived in advanced chemistry texts (31, 32), was later simplified to the commonly used van Deemter equation:

$$H = A + \frac{B}{\mu} + C\mu. \qquad 4.$$

Van Deemter et al. (13) presented a condensed form of the differential dependent on three empirical constants in contest with the mobile phase flow velocity (μ): eddy diffusion (A), diffusion (B), and mass transfer resistance (C). The van Deemter equation provides an accessible formula that relates the quality of a separation through plate height to clear empirical parameters such as column density and pressure. However, the stated equation offers little recognition of the underlying physical chemistry dictating the motion of a particle through a column and thus lacks true predictive power.

2.3. Stochastic Processes Model

Giddings & Eyring (14) approached the separation problem within a statistical framework based on the adsorption history of a molecule. The motion of each analyte molecule through a column is treated as a random walk between the mobile and stationary phases (**Figure 1*a***) (14, 33, 34). Total retention time (t_r) is then the sum of these transitions between the mobile and stationary phases, each lasting some time τ_j. Viewing the elution process in this manner provides a physical connection to the underlying chemistry lacking in the previous methods.

A fundamental assumption was made for their analysis in the form of the flow velocity of the mobile phase. The primary assertion, adopted by many of the theorists that followed, is that μ is constant throughout the length of the column (L). A corollary to this assumption is that the total time any analyte molecule spends in the mobile phase (t_0) is also constant, further reducing the complexity of the mathematics.

Combining constancy of these variables with the assumption of a linear isotherm means that the exact structure of the stationary phase can be neglected, as eddy currents are ignored and the distribution of site availability is averaged across the column. Instead, the variables of importance are the rate of adsorption and the number of times (n) that a molecule interacts with each type of site. The distribution of the number of adsorption events is then a Poisson distribution parameterized on the product $k_a * t_r$, where k_a is the adsorption rate constant, with the total elution time of an analyte molecule being as follows:

$$t_r = t_0 + \sum_i^{k_i} \sum_j^{n_j} \tau_j \ . \qquad 5.$$

Here, τ_j represents the adsorption time of the j-th adsorption on the i-th type of site. Equation 5 is an abstract template describing the time a molecule spends in the column as a sum of τ_j adsorption times across n adsorption events. The essence of the following theories is in identifying the number of adsorption distributions necessary to describe the column and to pull salient statistics from that information.

Giddings & Eyring's original paper (14) derived the probabilistic distribution of a single-site system and provided the framework to calculate it for any n-site system but provided only

the solution for a single-site column. Developments in the vein of the original theory sought to show equivalence between the stochastic processes model and other theories. Giddings (23) returned to this theory and derived solutions for a two-site system but found any further expansion intractable by then-current mathematical techniques. Denizot & Delaage (35) then proved that the probabilistic theory of Giddings was equivalent to the differential mass balance method, as both converged to the Gaussian elution profile, thereby uniting all theories.

2.4. Characteristic Functions

Characteristic functions (CFs) were posited by McQuarrie (36) to sidestep the complicated convolutions involved in addressing multisite adsorption, expanding on the theory of Giddings. Dondi & Remelli (24, 37) continued the development of CFs and showed that they could provide all the statistics necessary to fully describe an elution profile. CFs, and their subsequent use in Lévy processes, represent the current state of the stochastic theory (38).

A CF of a distribution is defined as the expectation $E[g(\xi)]$ of a function of the random variable ξ under the parent probability $F(x) = \Pr(\xi < x)$. This expectation is then equivalent to Equation 6a, where i represents the imaginary unit and $g(\xi) = \exp(\xi)$ (26):

$$\Phi(\xi) = \int \exp(i\xi x)\, f(x)\, \mathrm{d}x, \qquad 6a.$$

$$\Psi(\xi) = \ln[\Phi(\xi)]. \qquad 6b.$$

Equation 6a is commonly called the first CF. Equation 6b is the natural logarithm of the first CF and is called the second CF. The moments (u) [or cumulants (κ) for the second CF] are calculated from the derivatives of the CFs:

$$\Phi^{(j)}(0) = \left[\frac{\mathrm{d}^j \Phi(z)}{\mathrm{d}z^j}\right]_{z=0} = i^j u_j, \qquad 7a.$$

$$\Psi^{(j)}(0) = \left[\frac{\mathrm{d}^j \Psi(z)}{\mathrm{d}z^j}\right]_{z=0} = i^j \kappa_j. \qquad 7b.$$

In general, the CF of a distribution contains all the quantities necessary to recreate a Gaussian elution profile and to quantify the deviations from an ideal separation (24, 39). **Table 1** relates the cumulants of the second CF to many of these important statistical quantities. Inclusion of terms for dynamic flow speeds in the column and adaptations for systems with heterogeneous adsorption sites have been explored and point toward increased fidelity between theory and observation (40, 41).

Table 1 Cumulants of the second characteristic function (CF) and their statistical equivalents

Cumulant	Statistical equivalent	Chromatographic significance
κ_1	Mean, $\overline{m}$	Retention time, t_r
κ_2	Variance, σ^2	Variance of retention time
Coefficient 1	$\frac{\kappa_3}{\sigma^3}$	Skewness of elution peak
Coefficient 2	$\frac{\kappa_4}{\sigma^4}$	Excess of elution peak
NA	$(\frac{\sigma_r}{t_r})^2 L$	Plate height

Calculating the second CF of a chromatographic process can give the mean and variance of the retention time as well as quantify the asymmetry of the elution profile. Further, these values can be used to calculate the plate height when the standard deviation of the retention peak (σ_r) and the retention time (t_r) are calculated. Abbreviation: NA, not applicable. Data are from Reference 40.

2.5. Lévy Processes and Tailing

A natural extension of chromatographic theory is to model the trajectory of an analyte as a Lévy process (42, 43), yielding a quantitative description of elution tailing, a primary concern of chromatographic separations (**Figure 1*c***). Lévy processes define a system where the motion of an object undergoes many random and independent motions that are statistically identical across the time intervals of its trajectory. Under the Lévy model, the CF assumes the following form, where $\phi(\omega)$ represents the previous CFs cast into the frequency domain:

$$\phi(\omega) = \exp\left[i\omega t_m + t_m \int_0^\infty (\exp[i\omega\tau_s] - 1)\, M(d\tau_s) \right]. \quad 8.$$

Here, $M(d\tau_s)$ is the differential of the Lévy spectral function, which maps the number of adsorption steps that occur in the time between τ_s and $\tau_s + d\tau_s$ (38). Further, it should be noted that the inclusion of t_m incorporates a variability in the amount of time spent in the mobile phase, whereas t_0 assumes that all proteins spend the same amount of time in the column. This spectral function is recovered by taking the product of the cumulative distribution function $[F(\tau_s)]$ of adsorption time and the adsorption frequency (θ). Should the number of adsorption sites be sufficiently large and θ follow an exponential distribution, the Lévy model converges to the original Giddings–Eyring model (38).

Giddings (23) proposed that tailing is a kinetic effect driven by rare long binding events in the column, a position supported by later studies (40, 44). Probing how these rare binding sites are formed, and whether they are chemical in nature or are a result of structural differences, is an important question currently being explored (16, 45). Studies have shown that the theories presented are roughly equivalent in nature but still suffer from inaccuracies rooted in the mathematical assumptions made in each system (46–49). For example, averaging the mobile phase velocity, assuming a linear isotherm, and denoting the probability of adsorption as a constant are all approximations worthy of further investigation, especially in light of new advancements in probing individual molecules.

Modeling realistic chromatographic separations and pursuit of predictive column optimization is a growing field of research, spurred on by developments in single-molecule and super-resolution techniques (33). The benefit of the Lévy process approach is that there is a theoretical means to describe distributions of experimentally accessible parameters. While each trajectory is unique, there is a parent distribution with measurable ensemble statistics. Similarly, single-molecule studies identify individual analyte trajectories from a larger ensemble.

Further developments might include new terms to account for column heterogeneity, new distributions to describe adsorption mechanics, and better descriptions of molecular motion between adsorption events. Elucidating the contribution of each parameter and the necessary model adjustments requires examining the individual molecular trajectories and considering how an individual analyte's history contributes to the effects of a population. Such studies are ideally matched to the experimental methods pioneered in single-molecule and more recent super-resolution microscopies, many of which are described in the sections that follow.

3. SUPER-RESOLVED PROTEIN ADSORPTION AND DESORPTION

Single-molecule techniques close the knowledge gap between empirically established chromatographic theories with molecular-scale experimental observables (**Figure 2**). Molecular-scale details are acquired by directly monitoring individual analyte molecules, allowing access to intersite heterogeneities thought to be a major contributor to fronting and tailing in chromatographic

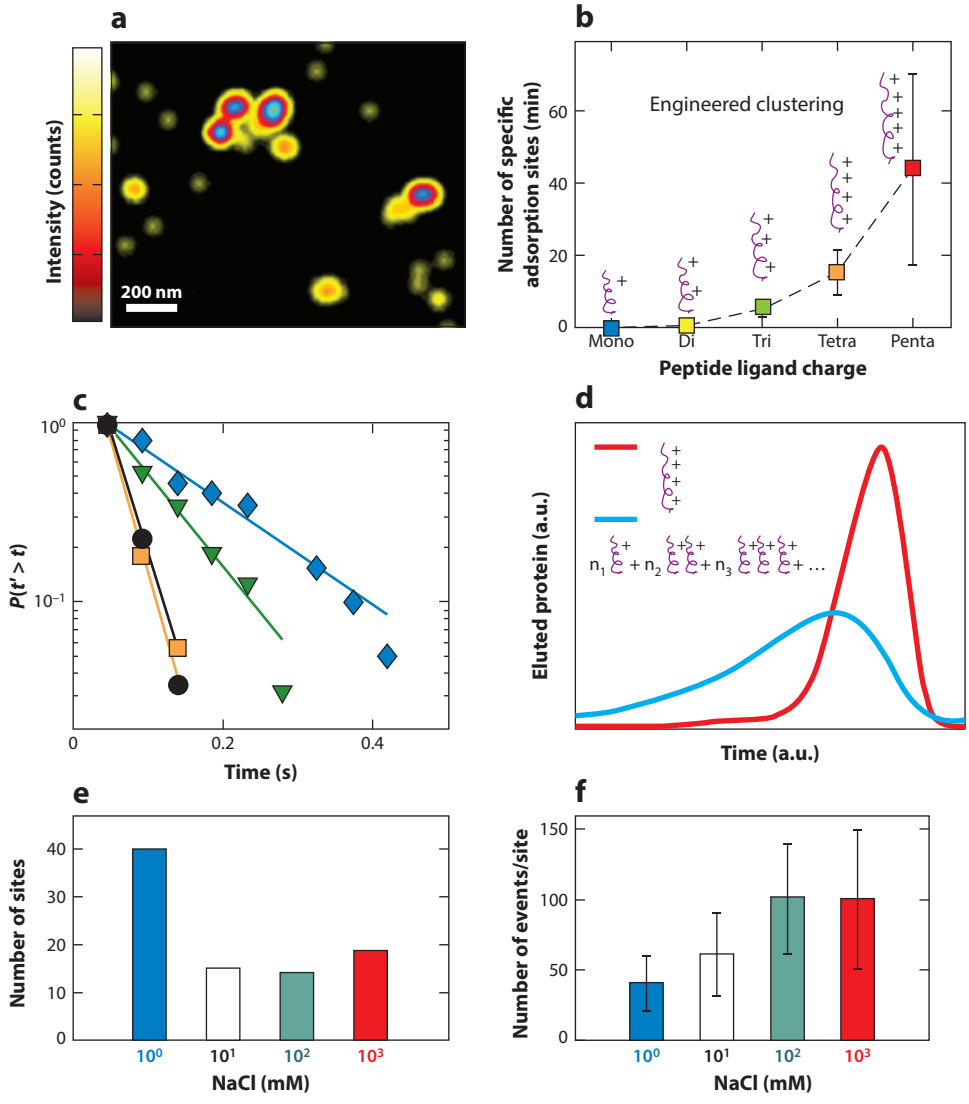

Figure 2

Eluting α-lactalbumin molecules from amide-functionalized agarose supports. (*a*) Specific adsorption sites are identified by super-resolving single adsorption events. (*b*) The number of identifiable specific adsorption sites increases with increasing oligomer length (shown with oligomer chains, *purple*). (*c*) Cumulative distributions of surface residence time of α-lactalbumin molecules from four different penta-charged sites, where *P* is the probability of adsorption event *t′* lasting longer than *t*. (*d*) Ensemble-averaged elution profiles for stochastically clustered monoargininamide–functionalized (1,706 sites; *blue*) and engineered pentaargininamide–functionalized (603 sites; *red*) agarose supports. (*e*,*f*) The number of specific adsorption sites decreases (*e*) while the number of total adsorption events per site increases (*f*) with increasing ionic strength in the mobile phase. Panels *a–d* adapted from Reference 50. Panels *e* and *f* adapted from Reference 45 with permission from Elsevier.

separations (32, 40, 44). Kisley et al. (50) investigated molecular-scale ion-exchange chromatography by utilizing fluorescently tagged α-lactalbumin and engineered agarose supports as a model system. α-Lactalbumin is a globular protein that carries a net negative charge under neutral pH, and agarose is a common porous support for the separation of biomolecules. For the experiments, agarose surfaces were functionalized with amide-containing ligands that carry net positive charges, thus forming a model ion-exchange system. Total internal reflection wide-field microscopy was used to observe the adsorption and desorption of proteins at ligand-functionalized sites on the stationary phase, while mobile-phase diffusion (diffusion coefficient ∼150 $\mu m^2/s$) was too fast to be observed. The experimenters achieved a sub-diffraction localization precision of ∼30 nm by fitting each adsorption event with a two-dimensional (2D) Gaussian function and extracting its spatial position as the centroid. Experimental details of the super-resolution experiment and analysis can be found in an extensive review of the subject (22, 51). Super-localization, coupled with kinetic analysis, made it possible to distinguish between specific, repeat protein adsorption at ligand sites and nonspecific adsorption due to trapping within pores on the agarose support (**Figure 2*a***).

One of the most important conclusions reached by the early super-resolved protein adsorption studies is that stochastic ligand clustering on the agarose support causes heterogeneity in protein adsorption-desorption kinetics (**Figure 2*b*–*d***). As suggested by Equation 5, adsorption heterogeneity leads directly to broadening of the macroscale elution time. The experiments showed that the underlying kinetics and associated macroscale elution profiles could be narrowed by engineering optimized ligand clusters (**Figure 2*b***) (50). Adsorption and desorption times were extracted at the single-site level by analyzing the waiting times between adsorption events and the residence times before desorption, respectively. Interestingly, even with optimized engineered ligand clusters, intersite heterogeneity for both adsorption and desorption was still observed (**Figure 2*c***).

Using the Lévy representation expressed in Equation 8, the distributions of protein desorption times were correlated to the ensemble elution profiles. Further comparison between the engineered sites versus the stochastically formed sites indicated that the HETP might be reduced by as much as fivefold by optimizing ligand clustering (50). A mathematical description of the separation efficiency was derived by converting the Poisson distribution of dwell times, extracted experimentally, to the following frequency domain relationship:

$$\phi\left(t_s;\omega\,|t_m\right)=\exp\left[r_m\sum_{i=1}^{i=k}\left(\left(\exp\left[i\omega\tau_{s,i}\right]-1\right)\Delta F\left(\tau_{s,i}\right)\right)\right]. \qquad 9.$$

In this equation, t_s is the time spent in the stationary phase, while t_m is the time spent in the mobile phase; r_m is the number of times a protein adsorbed during time t_m; and k is an index of the discrete set of desorption times. The elution profile can be extracted from a single-surface adsorption site with this equation. By taking all the specific adsorption sites into consideration and generating the site-averaged elution profiles, the difference between the stochastically clustered monoargininamide and pentaargininamide was obvious. The stochastically clustered monoargininamide resulted in more severe peak broadening, while the pentaargininamide exhibited a narrow Gaussian distribution with mild fronting (**Figure 2*d***). The theoretical plate heights were calculated by taking the ratio of the variances of the Gaussian fits to the peaks. It was found that the plate height of pentaargininamide-functionalized agarose was five times lower than the clustered monoargininamide-functionalized counterpart, indicating that the separation efficiency in chromatography can be much improved if proper surface engineering is performed.

The intersite kinetic heterogeneity in both adsorption and desorption (**Figure 2*c***) was later related to steric availability of ligand sites within the agarose stationary phase to the analyte proteins (45). Super-resolution imaging and kinetic analyses demonstrated that increasing ionic

strength both decreased heterogeneity in agarose pore size and narrowed the available sites on which proteins were observed to adsorb (45). Sodium chloride, with a concentration ranging from 1 to 1,000 mM, was added to the solution to adjust the ionic strength of the mobile phase. It was found that the number of specific adsorption sites was significantly reduced at increased salt concentrations (**Figure 2*e***), consistent with the notion that screening of electrostatic interactions by salt can eliminate most weakly accessible binding sites. However, the number of protein adsorption events at each remaining ligand site slightly increased with salt, an observation inconsistent with a purely electrostatic effect (**Figure 2*f***). Control experiments (not shown) suggested that instead, shrinking and narrowing of agarose pore sizes was also an important contributor to the observed protein–ligand interactions.

In ion-exchange separations, tuning ionic strength is a commonly used empirical parameter to optimize chromatographic elutions by influencing charge–charge interactions without significant effects on protein denaturation (52–54). Specifically, it is well established that high ionic strength in the mobile phase can reduce apparent adsorption heterogeneity, leading to higher eluting capabilities in ion-exchange chromatography (55, 56). However, the super-resolution and single-protein kinetic analyses discussed above demonstrate that the mechanisms driving the macroscale elution are more complex than can be explained by electrostatics alone. Simulation of macroscale elution profiles using Equation 9 predicted that separation could be enhanced threefold by suppressing steric heterogeneities among ligands (45).

Super-resolution studies, in addition to revealing the effects of ligand clustering and steric availability on specific adsorption at ligands, also provide insight about nonspecific protein adsorption to the stationary-phase support. Although specific adsorption sites are the dominating factor in the elution, contributions from nonspecific adsorption sites cannot be neglected. For example, the Wirth group and others (57–60) have shown that rare but long-lived adsorption to defects on silica stationary phases can have an outsized impact on the ensemble behavior. Shen et al. (61) studied the adsorption of α-lactalbumin onto thin nylon 6,6 films using wide-field single-molecule spectroscopy. The rate of protein adsorption was determined by counting the number of new adsorbed events per unit time per unit surface area. Under steady-state solution conditions, the rate of adsorption was found to be dependent on the time of adsorption and the protein concentration in the bulk solution. Super-resolution imaging analysis revealed that the surface-adsorbed protein molecules were at discrete nonspecific binding sites, which implied a monolayer adsorption model. A kinetic model was proposed allowing for extraction of the site-averaged rate constants for adsorption-desorption and the total number of adsorption sites on nylon surfaces. Comparing the protein adsorption on flat and porous nylon 6,6 films revealed that the porous structures increased the number of adsorption sites fourfold; however, the adsorption processes became less energetically favorable. Use of steady-state kinetic analyses can provide quantitative evaluation of the role of nonspecific adsorption on chromatographic performance.

Another important consideration when applying super-resolution methods to quantify adsorption and desorption dynamics is the limited temporal resolution of modern charge-coupled device detectors. Super temporal-resolved microscopy (STReM), recently developed by Wang et al. (19), demonstrated that it is possible to achieve temporal resolutions up to 20 times faster than common camera frame rates. This simple improvement allows for improved abilities to resolve fast events that are important in chromatographic separations (16, 62). Current detectable events have a lower bound of a few milliseconds, imposed by the camera frame rate. STReM adopts a concept from compressive sensing that makes it possible to encode fast subframe spatiotemporal information within a single frame (19). STReM is achieved by placing a double-helix phase mask (DHPM), originally designed for compressing 3D information into a 2D image (discussed further in Section 7) (63–65), into the optical detection path and rotating it at constant speed (19). Doing so encodes

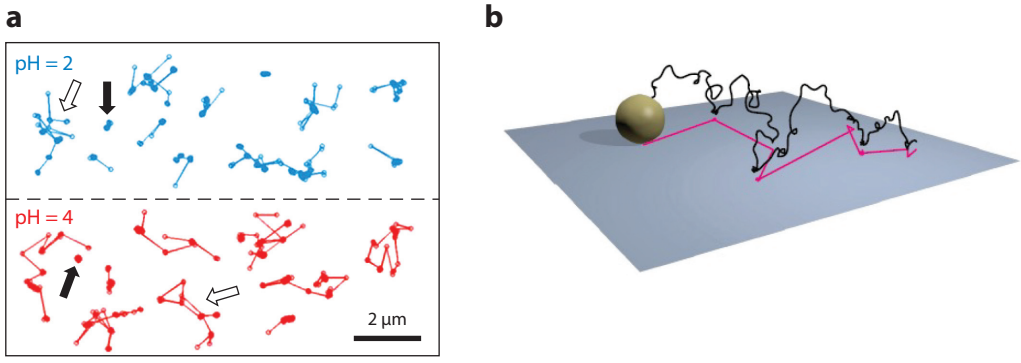

Figure 3

Molecular diffusions occurring on chromatographic supports. (*a*) Example trajectories for tracking the motions of single α-lactalbumin molecules under acidic conditions. Black arrows indicate examples of immobile α-lactalbumin molecules, and white arrows indicate surface-diffusing α-lactalbumin molecules. (*b*) Schematic illustration of a desorption-mediated continuous-time random walk. Panel *a* adapted from Reference 66 with permission from John Wiley and Sons. Panel *b* adapted from Reference 67 with permission from the American Physical Society.

subframe information into the orientations of the final double-helix (DH) point-spread functions (PSFs). The angular frequency is adjusted so that the DHPM rotates 180° in one frame; thus, the angle of the DHPM in a single frame encodes its subframe position. Using both simulated and experimental methods, it was shown that STReM can be applied to analytes that exhibit fast adsorption-desorption kinetics, have short subframe surface residence times, and even undergo subframe 2D transport (19). For the latter two scenarios, the resulting PSFs are complicated, and sophisticated analysis algorithms must be employed for data recovery (17). Nevertheless, STReM is capable of enhancing the effective temporal resolution by a factor of 20 in all three cases.

Single-molecule and super-resolution methods have recently revealed that protein adsorption-desorption can be coupled to additional processes that are not well described by simple physical models (16). Kisley et al. (66) studied α-lactalbumin adsorption at a silica substrate, a model system for aqueous normal-phase and hydrophilic interaction chromatography. Two linked modes of interaction were observed by single-molecule tracking under low pH conditions: adsorption-desorption and surface diffusion (**Figure 3*a***). It was suggested that such diffusive dynamics are a combination of electrostatic, hydrophobic, and hydrogen bonding interactions.

Schwartz and coworkers (67–70) have systematically studied protein interactions at various interfaces and proposed that the interaction could be modeled as a desorption-mediated continuous-time random walk (CTRW). Here, a CTRW means that an analyte molecule in the mobile phase intermittently hops through the bulk solution before stochastically immobilizing to a binding site for a variable amount of time (**Figure 3*b***) (67). Because the available adsorption sites are heterogeneous in binding energy, the waiting time of the CTRW is a broad distribution that can be expressed only by a power-law. CTRWs were widely observed over polymer matrices (68, 71), oil–water interfaces (69, 70), and functionalized substrates (72–74). These are usually considered as model substrates in reverse-phase liquid chromatography, normal-phase chromatography, and ion-exchange chromatography (57, 60). The preceding work suggests that protein adsorption-desorption at even the simplest chromatographic supports can be much more complicated than the equilibrium adsorption-desorption implicit within Langmuir adsorption models, but that super-resolution methods are useful for distinguishing, quantifying, and tuning the processes.

4. PROTEIN UNFOLDING AT STATIONARY-PHASE SUPPORTS

Reorganization of a protein's structural motif directly alters the intrinsic behavior, as the protein's size, geometry, overall charge, and exposed chemical domains are altered, thus introducing additional mechanisms to influence elutions (75, 76). Dynamic protein unfolding is a rich and complex field on its own, but it is important to consider the unique information that can be provided by single-molecule and super-resolution studies at stationary-phase surfaces. Importantly, single-molecule techniques allow for single proteins to be monitored in real time, thereby elucidating variations in dynamics of structural changes and surface dynamics and revealing otherwise hidden heterogeneities.

Single-molecule Förster resonance energy transfer (smFRET) is a technique that can be combined with single-particle tracking to measure nanometer-sized structural changes occurring in a protein during periods of transport and immobility at an adsorption site. The smFRET technique relies on nonradiative energy transfer, inversely proportional to the distance between two fluorescent probes, to measure distance changes on the order of nanometers (77–80), and it has been powerful in the investigation of protein structures at the single-molecule level in many systems discussed thoroughly elsewhere (81–86). The ability to interrogate conformational dynamics of proteins with molecular-scale precision has also been the result of advancements in fluorescent labeling techniques and methodologies, as discussed by Weiss and coworkers (87) and Yang & Yang (88). More recently, researchers have utilized smFRET combined with single-protein tracking to investigate protein dynamics at the interfaces of chromatographic support materials, uncovering mechanistic cues in protein unfolding pathways present in separation systems (89).

Kaar and coworkers (90) were the first to employ tracking smFRET to monitor protein conformational changes during interfacial adsorption, desorption, and surface diffusion dynamics. This work determined that two first-order kinetic pathways exist for the model protein organophosphorus hydrolase (OPH) to unfold on a fused silica (FS) interface. It was observed that if OPH unfolded during its trajectory at the FS interface, it could readily desorb regardless of its structural conformation during the initial adsorption. These findings provide proof that unfolded proteins can reversibly adsorb to an interface and likely result in solution-phase protein aggregates (91, 92). Kaar et al. were the first to show direct molecular-level evidence of this phenomenon, which likely serves as an initiation step in interfacial fouling. Studies indicate that fouling is predicated by the accumulation of unfolded proteins in the mobile phase of separation systems (90). This work highlights the strong potential of tracking smFRET to discern dynamics from conformational subpopulations of proteins during adsorption-desorption processes at stationary-phase supports, as well as to uncover the large discrepancy among protein unfolding timescales. Such details would traditionally not be accessible by ensemble-based measurements. Single-molecule measurements found evidence of transformations on the order of tenths of a second, compared to hour-long transformations detected by ensemble measurements. This discrepancy in timescales is likely due to ensemble measurements monitoring the relative rates to which unfolded and folded populations are changing in comparison to the unfolding processes of individual proteins in real time (90).

Further insights into unfolding and transport dynamics of proteins at industrially relevant support materials have been provided by tracking smFRET (93). Weltz and coworkers (94) investigated the transport and unfolding dynamics of a model protein lysozyme at a FS support. Tracking and unfolding trajectories shown in **Figure 4*a*** elucidated that lysozymes explore large amounts of the interface prior to unfolding. Lysozyme molecules exhibited a surface transport behavior consistent with a CTRW (95, 96), characterized by distinct hopping and waiting periods between adsorption sites along the support (**Figure 4*b***). Weltz and coworkers (94) determined that a rare subpopulation of adsorption sites exist on the support that induce lysozyme unfolding

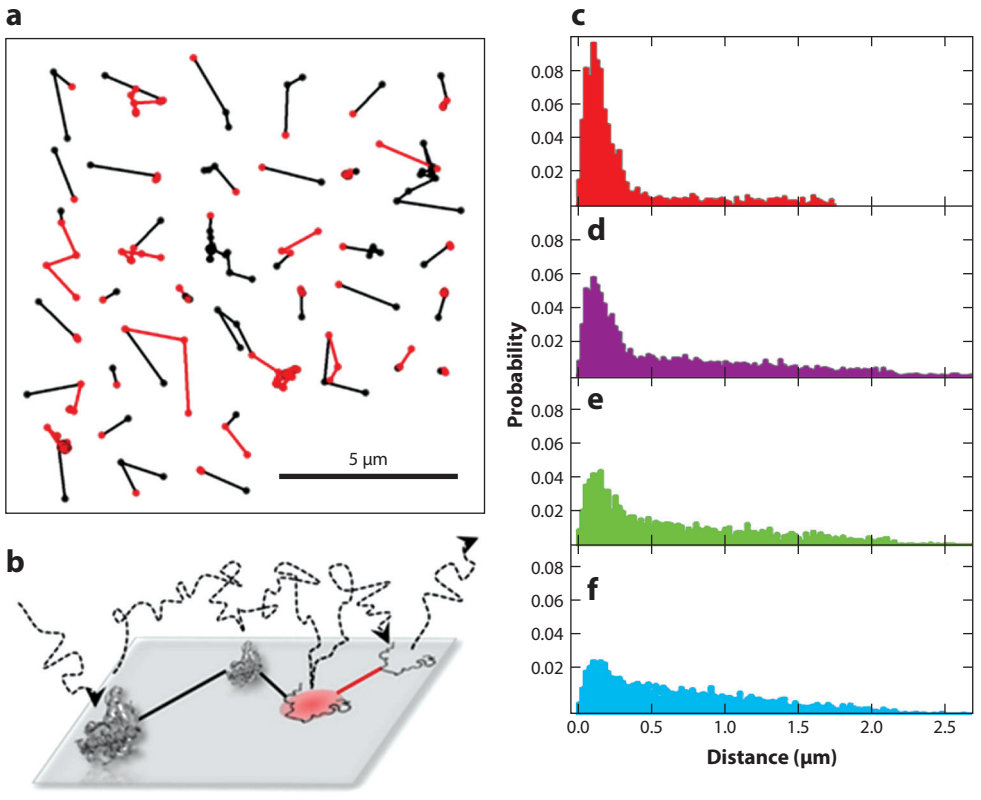

Figure 4

Lysozyme adsorption-unfolding dynamics on a FS (fused silica) stationary material. (*a*) Representative trajectories of lysozyme undergoing a search process for unfolding sites on the FS interface. Black segments of each trajectory represent the folded lysozyme state, and red segments indicate the unfolded conformation. (*b*) Schematic representation of proposed model behind surface-induced unfolding of lysozyme at unfolding sites. (*c–f*) Distributions of trajectories' Euclidean distance before first detected lysozyme unfolding event at total lysozyme concentrations of (*c*) 10×10^{-10} M, (*d*) 1.5×10^{-9} M, (*e*) 5.5×10^{-9} M, and (*f*) 7.1×10^{-8} M. Labeled lysozyme concentrations were held constant in panels *c–f*. Figure adapted from Reference 94 with permission from the American Chemical Society.

(**Figure 4*b***). In this study, the effective concentration of labeled lysozyme was fixed, while the amount of unlabeled lysozyme in the solution was increased incrementally in each experimental condition (**Figure 4*c–f***). It was determined that increasing the effective concentration and surface coverage of lysozyme caused labeled lysozyme molecules to explore larger distances on the support prior to unfolding on the surface (**Figure 4*c–f***). As a result of increasing the effective lysozyme concentration, the number of strongly adsorbing sites and the number of adsorptions at these sites decreased, thereby decreasing heterogeneity in the lysozyme–FS interactions. The decrease in heterogeneity was attributed to unlabeled lysozyme molecules passivating the surface at higher effective concentrations. Tracking results also highlighted that increasing the unlabeled lysozyme concentration caused the labeled lysozyme population to exhibit longer flights between adsorption sites and shorter waiting times between flights. These findings suggest that passivated support materials give rise to less heterogeneity in surface residence times of adsorbed protein

molecules and likely can mitigate resulting peak broadening in separation systems. Ultimately, this work highlights the importance of adsorption site heterogeneity and its direct role in protein unfolding and surface transport dynamics at support materials.

As discussed earlier, achieving greater temporal resolution is also important for understanding protein unfolding at a stationary support, given that unfolding dynamics can occur on fast timescales (97–99). Although tracking smFRET provides high-throughput acquisition of the unfolding and transport mechanics of model proteins, nontracking smFRET techniques can provide greater temporal resolution. For example, confocal-based smFRET can achieve microsecond temporal resolution (100). However, confocal smFRET exhibits lower throughput because of its smaller inherent imaging area. Saito and coworkers (100) utilized a confocal technique to uncover the unfolding dynamics of ubiquitin at a polymer-coated support. A covalent polymer coating was used to suppress artifacts originating from adsorption at the interface of the microfluidic assembly. The introduction of the hydrophobic polymer allowed for near-surface protein conformations to be measured with high temporal resolution. smFRET results indicated that ubiquitin exhibits a large heterogeneity in conformational states when unfolded. However, ubiquitin exhibits a well-defined structure while undergoing near-surface diffusion in the folded state. Interestingly, ubiquitin's structural changes in the unfolded states occurred on a timescale longer than 1 millisecond (100). These results provide insight into the complex nature of protein dynamics at a wide array of timescales unique to each protein and stationary phase.

Developing a more thorough understanding of protein unfolding dynamics at support interfaces is essential to optimizing separations through robust bottom-up design. The utility of smFRET for investigating real-time single-protein structural changes during surface transport at separation support materials has been discussed above. Advancements in labeling techniques, sensitive photon detectors, and experimental designs have allowed smFRET to be utilized in probing a large array of protein–surface interactions in real time. Although tradeoffs do exist between tracking and nontracking smFRET techniques, both provide access to fine details in the delicate and dynamic structural changes that occur in a protein while it is diffusing through separation systems. These techniques can be extended to more support materials and proteins to build on the already impressive fundamental understanding of the multifaceted processes of protein unfolding.

5. PROTEIN–PROTEIN INTERACTIONS

The target analyte protein is often only one of many proteins present in a separation column, providing another layer of complexity through potential protein–protein interactions. For example, mobile-phase interactions as well as competitive adsorption-desorption processes at the stationary phase can play a role in the overall performance of a separation system, although very little is known about the mechanistic details at the single-protein level. Many ensemble-based techniques have been utilized to investigate protein–protein interactions in a variety of systems and have been discussed thoroughly by Phizicky & Fields (101). In addition, a range of experimental (102, 103) and theoretical (104, 105) studies have explored how multiple proteins competitively adsorb to an interface. These processes are highly dynamic and play an important role in the separation of target proteins from upstream byproducts. Protein–protein and competitive protein adsorption effects should be investigated with single-molecule techniques in the future to develop a mechanistic understanding of these processes. Recently, Kisley et al. (106) reported that insulin competitors in the mobile phase blocked α-lactalbumin adsorption at some ligands but had no influence on adsorption/desorption kinetics at sites where adsorption did occur. This unexpected result certainly merits further experimental and theoretical examination.

6. PROTEIN TRANSPORT AT POROUS SUPPORTS

Chromatographic separations utilize porous stationary-phase materials that introduce many complex paths for proteins to explore during elution. Porous surface features are often heterogeneous in size, density, and overall surface morphology (107). Protein translation and rotation within pores can be hindered under nanoconfined conditions. This complexity presents a challenge to experimental quantification of structure–function relationships present in separation systems. Porous polymer supports are increasingly commonplace because of their low fabrication price, chemical stability, and ease of surface functionalization (108–110). Studying protein interactions with porous supports via super-resolution microscopy provides structural details of porous networks and dynamic information about protein transport simultaneously.

The development of noninvasive techniques to report structure–function relationships in separation systems is essential to the development of function-specific support materials. Advanced imaging techniques such as atomic force microscopy and scanning electron microscopy are able to image porous structure with nanometer-scale spatial resolution. However, these methods can damage delicate polymer materials during image acquisition and have limited functionality in quantifying dynamics under the aqueous conditions necessary for protein separations (111). In particular, porous supports can reversibly swell and shrink in the changing ion-exchange solution conditions (112). An ideal experimental technique would provide in situ imaging of porous supports in tandem with single-molecule tracking, allowing insights into the relationship between underlying structure of support materials and analyte protein transport dynamics (113, 114). Of particular utility is the recently developed fluorescence correlation spectroscopy super-resolution optical fluctuation imaging (fcsSOFI) method (115).

fcsSOFI enables both the porous substrate morphology and the particle transport kinetics to be simultaneously quantified by relating fluorescence fluctuations due to hindered diffusion within a pore to the size of the pore (115). fcsSOFI has the potential to provide rich sub-diffraction information in environments where emitter signals are low and/or in confined spaces (116–118). Mathematically, fcsSOFI generates a high-resolution image of the porous support from an autocorrelation map (115). The super-resolved image is calculated from the second-order autocorrelation of each pixel (119). Each PSF in the second-order autocorrelation map is spatially enhanced by a factor related to the diffusion coefficient:

$$G_2(r,\tau) \sim \int \mathrm{d}r_1 U(r-r_1) \times \left[U(r-r_1) \otimes \exp\left(-\frac{(r-r_1)^2}{4D\tau} \right) \right] \varepsilon_1 \varepsilon_2, \qquad 10.$$

in which $U(r)$ represents the PSF distribution, ε_1 and ε_2 are the constant brightness of an emitter in two consecutive frames, D denotes the diffusion coefficient from fluorescence correlation spectroscopy, τ represents a time lag, and $\otimes$ is the convolution operation. The PSF in the autocorrelation map is enhanced to a spatial resolution below the optical diffraction limit:

$$\frac{1}{\sigma^2_{\mathrm{new}}} = \frac{1}{\sigma^2_{xy}} + \frac{1}{\sigma^2_{xy} + nD\tau},$$

in which n is a constant determined by the dimensions of the emitter movement and σ is the standard deviation of the PSF's Gaussian. The resolution of a fcsSOFI image is thus improved by a factor between 0 and $\sqrt{2}$.

Kisley et al. (115) demonstrated the utility of this technique in both simulated and experimental systems. In this work, a 1D transport simulation is performed, and the pore structure is recovered with a high spatial resolution. **Figure 5*a*** illustrates how the diffusion coefficient is calculated by fitting the autocorrelation curve. Results are compared to ground truth data and achieve an

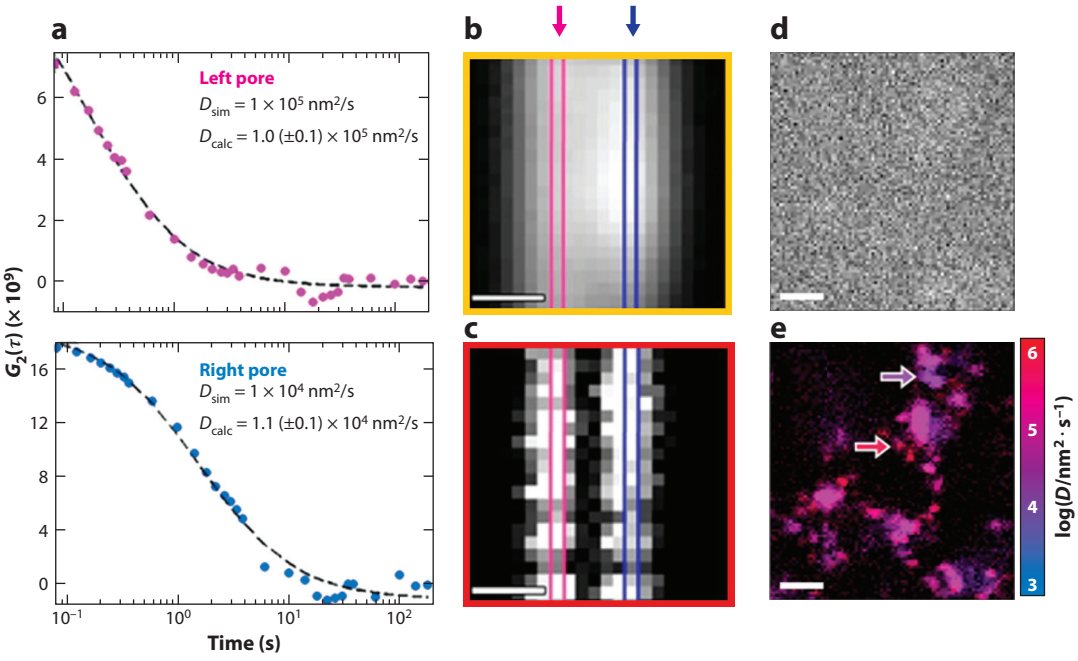

Figure 5

Protein separation study on porous substrate using fluorescence correlation spectroscopy super-resolution optical fluctuation imaging (fcsSOFI). (*a*) Extracting the diffusion coefficient D from simulated 1D diffusion with fcsSOFI. G_2 is defined as in Equation 10. (*b*) Simulated frame-averaged image of emitter diffusion in two pores located within the diffraction limit of each other. True pore positions are labeled by arrows. (*c*) The pore structure resolved with second-order fcsSOFI calculation and one step of blind deconvolution. (*d*,*e*) Diffusion coefficient distribution and pore size from (*d*) diffraction-limited image and (*e*) fcsSOFI image of 1% agarose structure. (*b*–*e*) Scale bar = 2 μm. Figure adapted from Reference 115 with permission from the American Chemical Society.

error under 10%. Second-order autocorrelation allows for spatial resolution beyond the optical diffraction limit (**Figure 5*b***) and can be used to recover the substrate structure (**Figure 5*c***). Experimentally, Kisley et al. applied fcsSOFI to image a porous agarose support as a model system due to its use as a stationary support in separation systems. As compared to the raw image (**Figure 5*d***), fcsSOFI images can resolve heterogeneities in agarose pore size and relate them to transport dynamics of analytes within the pores (**Figure 5*e***). The ability to resolve both the porous structure of agarose and the dynamics of an emitter in an aqueous environment was an essential advancement in resolving real-time transport in these complex support materials. In the same work, fcsSOFI was successfully applied to resolve the structure of lyotropic liquid crystal gels using perylene diimide as the reporter molecule, achieving results not obtainable with traditional single-particle tracking (SPT). The versatility and robustness of fcsSOFI suggest that it will prove an essential tool in developing a fundamental understanding of the structure–function relationships underlying separations at porous supports.

7. 3D SUPER-RESOLVED PROTEIN INTERACTIONS AT POROUS SUPPORTS

A method of directly measuring a protein's interaction in porous supports with high axial and lateral spatial resolution would provide unprecedented detail about protein separation systems.

3D protein transport in porous materials is not completely captured with other types of super-resolution imaging because all output images and diffusion maps are projected onto a 2D plane. In comparison, 3D super-resolution microscopy is a powerful tool for studying protein kinetics on porous substrates (15, 64, 120) and can be achieved using multifocal plane microscopy (121, 122), astigmatic imaging using a cylindrical lens (123, 124), light-sheet fluorescent microscopy (125, 126), or DH PSF microscopy (63, 64). Here, we focus on DH PSF 3D microscopy, originally proposed by Pavani & Piestun (65) as a route for providing high spatial resolution and localization of fluorescent emitters in 3D. We emphasize this technique because of its simplistic implementation in existing microscopy setups, high spatial localization capability, and larger axial range compared with other 3D super-resolution microscopy techniques (127). DH PSF microscopy provides 3D localization of a fluorescent emitter by the addition of a 4*f* system (128) and a DHPM (65) in the detection path of a traditional microscope (**Figure 6*a***). The addition of the phase mask within the 4*f* system causes the 2D Gaussian PSF to be converted to a DH PSF that has two lobes (**Figure 6*b***).

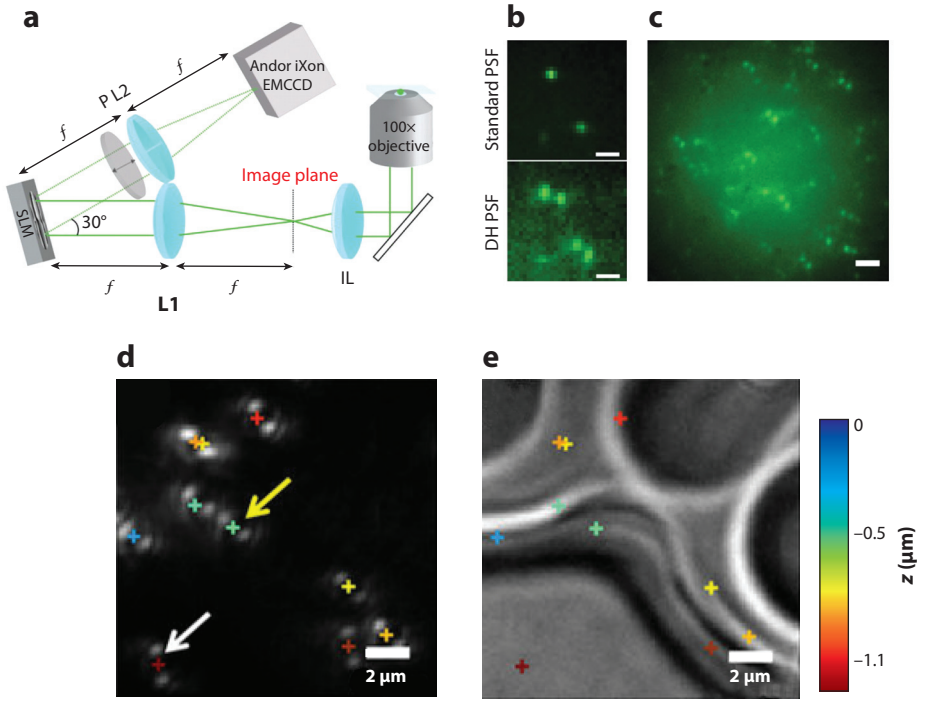

Figure 6

Application of DH PSF microscopy to the study of a porous substrate. (*a*) Scheme of DH PSF 3D microscopy. (*b*) Representative data of standard PSF and DH PSF. (*c*) DCDHF-P fluorophore molecules diffusing in a thick PMMA polymer substrate. (*d*) Localization of fluorescent beads in 3D on a porous polystyrene film by fitting the DH PSF. The white arrow indicates an emitter residing in a pore, and the yellow arrow indicates an emitter on the top of a pore wall with resulting DH PSF orientations. (*e*) Overlay of 3D localization on the bright-field image of the porous polystyrene film shown in panel *d*. (*b–e*) Scale bar = 2 µm. Abbreviations: DCDHF-P, *para*-2-dicyanomethylene-3-cyano-2,5-dihydrofuran; DH PSF, double-helix point-spread function; EMCCD, electron-multiplying charge-coupled device; IL, imaging lens; L1, lens 1; L2, lens 2; P, polarizer; PMMA, poly(methyl methacrylate); SLM, spatial light modulator. Panels *a–c* adapted from Reference 64. Panels *d* and *e* adapted from Reference 17 with permission.

The orientation of the two lobes encodes the depth of the emitters. Doing so provides a spatial resolution of ~20 nm in both the lateral and axial dimensions (64).

3D SPT is a powerful tool to provide insight into the interaction of molecules on a porous substrate. Pavani and coworkers (64) first applied DH microscopy to track DCDHF-P fluorophore molecules in a thick poly(methyl methacrylate) (PMMA) polymer surface (**Figure 6*c***). They reported that the diffusion of single fluorescent emitters can be distinguished in 3D below the diffraction limit (64). In addition, Shuang et al. (17) studied the adsorption and desorption of fluorescent beads on porous polystyrene films. Varied orientation of the DH PSF lobes encodes adsorption site depths (**Figure 6*d***). Overlaying the single-molecule localizations on a bright-field image of the underlying porous surface provided confirmation of the axial resolution of this technique on porous polymer supports (**Figure 6*e***). Improved resolution in 3D makes DH microscopy an invaluable tool in the analysis and investigation of porous media.

We know of no published studies utilizing DH microscopy to investigate 3D protein dynamics at realistic stationary-phase supports as of yet, but the technique's utility for studying chromatographic systems is clear. The ability to fully resolve a protein's transport through a column comprised of functionalized porous stationary-phase material is essential to achieving predictive chromatography.

8. CONCLUSION

We discussed the current state of chromatographic theories and assumptions that are made in each respective theory. Next, we provided the current outlook of super-resolution techniques and their implementation for investigating three main components of separation systems: adsorption-desorption dynamics, protein unfolding and competitive protein kinetics, and transport in porous stationary-phase media. We highlighted super-resolution microscopy's ability to provide mechanistic insights into the heterogeneous behaviors of protein molecules' interactions in separation systems, and most importantly to extract parameters that can be directly related to a stochastic theory. We forecast that super-resolution techniques will continue to provide mechanistic insights into the complex components in chromatographic systems and will yield, eventually, a robust and predictive theory of chromatographic separations.

DISCLOSURE STATEMENT

The authors are not aware of any affiliations, memberships, funding, or financial holdings that might be perceived as affecting the objectivity of this review.

ACKNOWLEDGMENTS

This work was funded by the National Science Foundation (CBET-1438634) and the Welch Foundation (C1787). Also, N.A.M. acknowledges that this material is based upon work supported by the National Science Foundation Graduate Research Fellowship Program (grant 1450681).

LITERATURE CITED

1. Avorn J. 2015. The $2.6 billion pill—methodologic and policy considerations. *N. Engl. J. Med.* 372:1877–79
2. Ahuja S, ed. 2000. *Handbook of Bioseparations*. London: Academic
3. Brady R, Woonton B, Gee ML, O'Connor AJ. 2008. Hierarchical mesoporous silica materials for separation of functional food ingredients—a review. *Innov. Food Sci. Emerg. Technol.* 9:243–48

4. BioPlan Assoc. 2017. *Annual report and survey of biopharmaceutical manufacturing capacity and production*. BioPlan Assoc., Rockville, MD
5. Thömmes J, Kula MR. 1995. Membrane chromatography—an integrative concept in the downstream processing of proteins. *Biotechnol. Prog.* 11:357–67
6. Shukla AA, Hubbard B, Tressel T, Guhan S, Low D. 2007. Downstream processing of monoclonal antibodies—application of platform approaches. *J. Chromatogr. B* 848:28–39
7. Lowe CR, Lowe AR, Gupta G. 2001. New developments in affinity chromatography with potential application in the production of biopharmaceuticals. *J. Biochem. Biophys. Methods* 49:561–74
8. McGrath NA, Brichacek M, Njardarson JT. 2010. A graphical journey of innovative organic architectures that have improved our lives. *J. Chem. Educ.* 87:1348–49
9. Butcher L. 2011. Employers struggle to cope with the rising use of biologics: tradeoffs in cost sharing or higher deductibles could derail treatment and decrease the value of healthcare spending. *Biotechnol. Healthc.* 8:21–24
10. Walsh G. 2014. Biopharmaceutical benchmarks. *Nat. Biotechnol.* 32:992–1000
11. Murch D. 1953. Height of equivalent theoretical plate in packed fractionation columns. *Ind. Eng. Chem.* 45:2616–21
12. Peters WA. 1923. Calculations on fractionating columns from theoretical data. *Ind. Eng. Chem.* 15:402–3
13. van Deemter JJ, Zuiderweg FJ, Klinkenberg A. 1956. Longitudinal diffusion and resistance to mass transfer as causes of nonideality in chromatography. *Chem. Eng. Sci.* 5:271–89
14. Giddings JC, Eyring H. 1955. A molecular dynamic theory of chromatography. *J. Phys. Chem.* 59:416–21
15. von Diezmann A, Shechtman Y, Moerner WE. 2017. Three-dimensional localization of single molecules for super-resolution imaging and single-particle tracking. *Chem. Rev.* 117:7244–75
16. Kisley L, Landes CF. 2014. Molecular approaches to chromatography using single molecule spectroscopy. *Anal. Chem.* 87:83–98
17. Shuang B, Wang W, Shen H, Tauzin LJ, Flatebo C, et al. 2016. Generalized recovery algorithm for 3D super-resolution microscopy using rotating point spread functions. *Sci. Rep.* 6:30826
18. Shuang B, Chen J, Kisley L, Landes CF. 2014. Troika of single particle tracking programing: SNR enhancement, particle identification, and mapping. *Phys. Chem. Chem. Phys.* 16:624–34
19. Wang W, Shen H, Shuang B, Hoener BS, Tauzin LJ, et al. 2016. Super temporal-resolved microscopy (STReM). *J. Phys. Chem. Lett.* 7:4524–29
20. Shuang B, Byers CP, Kisley L, Wang LY, Zhao JL, et al. 2013. Improved analysis for determining diffusion coefficients from short, single-molecule trajectories with photoblinking. *Langmuir* 29:228–34
21. Cho N-J, Frank CW, Kasemo B, Höök F. 2010. Quartz crystal microbalance with dissipation monitoring of supported lipid bilayers on various substrates. *Nat. Protoc.* 5:1096–106
22. Shen H, Tauzin LJ, Baiyasi R, Wang W, Moringo N, et al. 2017. Single particle tracking: from theory to biophysical applications. *Chem. Rev.* 117:7331–76
23. Giddings JC. 1963. Kinetic origin of tailing in chromatography. *Anal. Chem.* 35:1999–2002
24. Dondi F, Remelli M. 1986. The characteristic function method in the stochastic theory of chromatography. *J. Phys. Chem.* 90:1885–91
25. Giddings JC. 1965. *Dynamics of Chromatography: Principles and Theory*. New York: Dekker
26. Cramér H. 1946. *Mathematical Methods of Statistics*. Princeton, NJ: Princeton Univ. Press
27. Martin AJP, Synge RLM. 1941. A new form of chromatogram employing two liquid phases. *Biochem. J.* 35:1358–68
28. Lapidus L, Amundson NR. 1952. Mathematics of adsorption in beds. IV. The effect of longitudinal diffusion in ion exchange and chromatographic columns. *J. Phys. Chem.* 56:984–88
29. Chandra N, Brew K, Acharya KR. 1998. Structural evidence for the presence of a secondary calcium binding site in human α-lactalbumin. *Biochemistry* 37:4767–72
30. Said AS. 1981. *Theory and Mathematics of Chromatography*. Heidelberg, Ger.: Hüthig
31. Felinger A. 1998. *Data Analysis and Signal Processing in Chromatography*. Amsterdam: Elsevier
32. Guiochon G, Felinger A, Shirazi DG. 2006. *Fundamentals of Preparative and Nonlinear Chromatography*. Amsterdam: Elsevier
33. Felinger A. 2008. Molecular dynamic theories in chromatography. *J. Chromatogr. A* 1184:20–41

34. Giddings JC. 1958. The random downstream migration of molecules in chromatography. *J. Chem. Educ.* 35:588
35. Denizot FC, Delaage MA. 1975. Statistical theory of chromatography: new outlooks for affinity chromatography. *PNAS* 72:4840–43
36. McQuarrie DA. 1963. On the stochastic theory of chromatography. *J. Chem. Phys.* 38:437–45
37. Dondi F, Remelli M. 1984. Characterization of extracolumn and concentration-dependent distortion of chromatographic peaks by Edgeworth–Cramér series. *J. Chromatogr.* 315:67–73
38. Dondi F, Cavazzini A, Pasti L. 2006. Chromatography as Lévy stochastic process. *J. Chromatogr. A* 1126:257–67
39. Dondi F. 1982. Approximation properties of the Edgeworth–Cramér series and determination of peak parameters of chromatographic peaks. *Anal. Chem.* 54:473–77
40. Cavazzini A, Remelli M, Dondi F. 1997. Stochastic theory of two-site adsorption chromatography by the characteristic function method. *J. Microcolumn Sep.* 9:295–302
41. Dondi F, Cavazzini A, Remelli M. 1998. The stochastic theory of chromatography. *Adv. Chromatogr.* 38:51–74
42. Asmussen S. 2014. Lévy processes, phase-type distributions, and martingales. *Stoch. Models* 30:443–68
43. Pasti L, Marchetti N, Guzzinati R, Catani M, Bosi V, et al. 2016. Microscopic models of liquid chromatography: from ensemble-averaged information to resolution of fundamental viewpoint at single-molecule level. *Trends Anal. Chem.* 81:63–68
44. Cavazzini A, Remelli M, Dondi F, Felinger A. 1999. Stochastic theory of multiple-site linear adsorption chromatography. *Anal. Chem.* 71:3453–62
45. Kisley L, Chen JX, Mansur AP, Dominguez-Medina S, Kulla E, et al. 2014. High ionic strength narrows the population of sites participating in protein ion-exchange adsorption: a single-molecule study. *J. Chromatogr. A* 1343:135–42
46. Bacskay I, Felinger A. 2009. Macroscopic and microscopic analysis of mass transfer in reversed phase liquid chromatography. *J. Chromatogr. A* 1216:1253–62
47. Felinger A, Cavazzini A, Dondi F. 2004. Equivalence of the microscopic and macroscopic models of chromatography: stochastic-dispersive versus lumped kinetic model. *J. Chromatogr. A* 1043:149–57
48. Cavazzini A, Dondi F, Jaulmes A, Vidal-Madjar C, Felinger A. 2002. Monte Carlo model of nonlinear chromatography: correspondence between the microscopic stochastic model and the macroscopic Thomas kinetic model. *Anal. Chem.* 74:6269–78
49. Felinger A, Guiochon G. 2004. Comparison of the kinetic models of linear chromatography. *Chromatographia* 60:S175–80
50. Kisley L, Chen J, Mansur AP, Shuang B, Kourentzi K, et al. 2014. Unified superresolution experiments and stochastic theory provide mechanistic insight into protein ion-exchange adsorptive separations. *PNAS* 111:2075–80
51. Small A, Stahlheber S. 2014. Fluorophore localization algorithms for super-resolution microscopy. *Nat. Methods* 11:267–79
52. Lan Q, Bassi AS, Zhu J-X, Margaritis A. 2001. A modified Langmuir model for the prediction of the effects of ionic strength on the equilibrium characteristics of protein adsorption onto ion exchange/affinity adsorbents. *Chem. Eng. J.* 81:179–86
53. Cano T, Offringa ND, Willson RC. 2005. Competitive ion-exchange adsorption of proteins: competitive isotherms with controlled competitor concentration. *J. Chromatogr. A* 1079:116–26
54. Chang C, Lenhoff AM. 1998. Comparison of protein adsorption isotherms and uptake rates in preparative cation-exchange materials. *J. Chromatogr. A* 827:281–93
55. Yamamoto S, Nakanishi K, Matsuno R. 1988. *Ion-Exchange Chromatography of Proteins*. New York: Dekker
56. Kato K, Ikada Y. 1995. Selective adsorption of proteins to their ligands covalently immobilized onto microfibers. *Biotechnol. Bioeng.* 47:557–66
57. Wirth MJ, Swinton DJ. 1998. Single-molecule probing of mixed-mode adsorption at a chromatographic interface. *Anal. Chem.* 70:5264–71
58. Wirth MJ, Swinton DJ, Ludes MD. 2003. Adsorption and diffusion of single molecules at chromatographic interfaces. *J. Phys. Chem. B* 107:6258–68

59. Mabry JN, Skaug MJ, Schwartz DK. 2014. Single-molecule insights into retention at a reversed-phase chromatographic interface. *Anal. Chem.* 86:9451–58
60. Wirth MJ, Legg MA. 2007. Single-molecule probing of adsorption and diffusion on silica surfaces. *Annu. Rev. Phys. Chem.* 58:489–510
61. Shen H, Tauzin LJ, Wang W, Hoener B, Shuang B, et al. 2016. Single-molecule kinetics of protein adsorption on thin nylon-6,6 films. *Anal. Chem.* 88:9926–33
62. Fanali S, Haddad PR, Poole C, Riekkola ML. 2017. *Liquid Chromatography: Fundamentals and Instrumentation*. Amsterdam: Elsevier
63. Pavani SRP, Piestun R. 2009. *3D fluorescent particle tracking with nanometer scale accuracies using a double-helix point spread function*. Presented at Conf. Lasers Electro-Opt./Int. Conf. Quantum Electron., May 31–June 5, Baltimore, MD
64. Pavani SRP, Thompson MA, Biteen JS, Lord SJ, Liu N, et al. 2009. Three-dimensional, single-molecule fluorescence imaging beyond the diffraction limit by using a double-helix point spread function. *PNAS* 106:2995–99
65. Pavani SRP, Piestun R. 2008. High-efficiency rotating point spread functions. *Opt. Express* 16:3484–89
66. Kisley L, Poongavanam MV, Kourentzi K, Willson RC, Landes CF. 2016. pH-dependence of single-protein adsorption and diffusion at a liquid chromatographic interface. *J. Sep. Sci.* 39:682–88
67. Skaug MJ, Mabry J, Schwartz DK. 2013. Intermittent molecular hopping at the solid–liquid interface. *Phys. Rev. Lett.* 110:256101
68. Wang D, Chin H-Y, He C, Stoykovich MP, Schwartz DK. 2016. Polymer surface transport is a combination of in-plane diffusion and desorption-mediated flights. *ACS Macro Lett.* 5:509–14
69. McUmber AC, Larson NR, Randolph TW, Schwartz DK. 2015. Molecular trajectories provide signatures of protein clustering and crowding at the oil/water interface. *Langmuir* 31:5882–90
70. Wang DP, Hu RF, Mabry JN, Miao B, Wu DT, et al. 2015. Scaling of polymer dynamics at an oil–water interface in regimes dominated by viscous drag and desorption-mediated flights. *J. Am. Chem. Soc.* 137:12312–20
71. Tauzin LJ, Shuang B, Kisley L, Mansur AP, Chen J, et al. 2014. Charge-dependent transport switching of single molecular ions in a weak polyelectrolyte multilayer. *Langmuir* 30:8391–99
72. Tauzin LJ, Shen H, Moringo NA, Roddy MH, Bothof CA, et al. 2016. Variable surface transport modalities on functionalized nylon films revealed with single molecule spectroscopy. *RSC Adv.* 6:27760–66
73. Giri D, Ashraf KM, Collinson MM, Higgins DA. 2015. Single-molecule perspective on mass transport in condensed water layers over gradient self-assembled monolayers. *J. Phys. Chem. C* 119:9418–28
74. Sukhishvili SA, Granick S. 1999. Adsorption of human serum albumin: dependence on molecular architecture of the oppositely charged surface. *J. Chem. Phys.* 110:10153–61
75. McNay JL, Fernandez EJ. 1999. How does a protein unfold on a reversed-phase liquid chromatography surface? *J. Chromatogr. A* 849:135–48
76. Benedek K, Dong S, Karger B. 1984. Kinetics of unfolding of proteins on hydrophobic surfaces in reversed-phase liquid chromatography. *J. Chromatogr. A* 317:227–43
77. Ha T, Enderle T, Ogletree D, Chemla DS, Selvin PR, Weiss S. 1996. Probing the interaction between two single molecules: fluorescence resonance energy transfer between a single donor and a single acceptor. *PNAS* 93:6264–68
78. Roy R, Hohng S, Ha T. 2008. A practical guide to single-molecule FRET. *Nat. Methods* 5:507–16
79. Weiss S. 1999. Fluorescence spectroscopy of single biomolecules. *Science* 283:1676–83
80. Darugar Q, Kim H, Gorelick RJ, Landes C. 2008. Human T-cell lymphotropic virus type 1 nucleocapsid protein-induced structural changes in transactivation response DNA hairpin measured by single-molecule fluorescence resonance energy transfer. *J. Virol.* 82:12164–71
81. Shaikh SA, Dolino DM, Lee G, Chatterjee S, MacLean DM, et al. 2016. Stargazin modulation of AMPA receptors. *Cell Rep.* 17:328–35
82. Cooper DR, Dolino DM, Jaurich H, Shuang B, Ramaswamy S, et al. 2015. Conformational transitions in the glycine-bound GluN1 NMDA receptor LBD via single-molecule FRET. *Biophys. J.* 109:66–75
83. Chen JX, Poddar NK, Tauzin LJ, Cooper D, Kolomeisky AB, Landes CF. 2014. Single-molecule FRET studies of HIV TAR-DNA hairpin unfolding dynamics. *J. Phys. Chem. B* 118:12130–39

84. Kisley L, Serrano KA, Guin D, Kong X, Gruebele M, Leckband DE. 2017. Direct imaging of protein stability and folding kinetics in hydrogels. *ACS Appl. Mater. Interfaces* 9:21606–17
85. Chen T-Y, Santiago AG, Jung W, Krzemiński Ł, Yang F, et al. 2015. Concentration-and chromosome-organization-dependent regulator unbinding from DNA for transcription regulation in living cells. *Nat. Commun.* 6:7445
86. Ramaswamy S, Cooper D, Poddar N, MacLean DM, Rambhadran A, et al. 2012. Role of conformational dynamics in α-amino-3-hydroxy-5-methylisoxazole-4-propionic acid (AMPA) receptor partial agonism. *J. Biol. Chem.* 287:43557–64
87. Jäger M, Nir E, Weiss S. 2006. Site-specific labeling of proteins for single-molecule FRET by combining chemical and enzymatic modification. *Protein Sci.* 15:640–46
88. Yang J-Y, Yang WY. 2009. Site-specific two-color protein labeling for FRET studies using split inteins. *J. Am. Chem. Soc.* 131:11644–45
89. Faulón Marruecos D, Kastantin M, Schwartz DK, Kaar JL. 2016. Dense poly(ethylene glycol) brushes reduce adsorption and stabilize the unfolded conformation of fibronectin. *Biomacromolecules* 17:1017–25
90. McLoughlin SY, Kastantin M, Schwartz DK, Kaar JL. 2013. Single-molecule resolution of protein structure and interfacial dynamics on biomaterial surfaces. *PNAS* 110:19396–401
91. Felsovalyi F, Patel T, Mangiagalli P, Kumar SK, Banta S. 2012. Effect of thermal stability on protein adsorption to silica using homologous aldo-keto reductases. *Protein Sci.* 21:1113–25
92. Felsovalyi F, Mangiagalli P, Bureau C, Kumar SK, Banta S. 2011. Reversibility of the adsorption of lysozyme on silica. *Langmuir* 27:11873–82
93. Langdon BB, Kastantin M, Schwartz DK. 2015. Surface chemistry influences interfacial fibrinogen self-association. *Biomacromolecules* 16:3201–8
94. Weltz JS, Schwartz DK, Kaar JL. 2015. Surface-mediated protein unfolding as a search process for denaturing sites. *ACS Nano* 10:730–38
95. Fisher ME, Kolomeisky AB. 1999. Molecular motors and the forces they exert. *Physica A* 274:241–66
96. Kastantin M, Langdon BB, Chang EL, Schwartz DK. 2011. Single-molecule resolution of interfacial fibrinogen behavior: effects of oligomer populations and surface chemistry. *J. Am. Chem. Soc.* 133:4975–83
97. Chung HS, Louis JM, Eaton WA. 2009. Experimental determination of upper bound for transition path times in protein folding from single-molecule photon-by-photon trajectories. *PNAS* 106:11837–44
98. Nettels D, Hoffmann A, Schuler B. 2008. Unfolded protein and peptide dynamics investigated with single-molecule FRET and correlation spectroscopy from picoseconds to seconds. *J. Phys. Chem. B* 112:6137–46
99. Nettels D, Gopich IV, Hoffmann A, Schuler B. 2007. Ultrafast dynamics of protein collapse from single-molecule photon statistics. *PNAS* 104:2655–60
100. Saito M, Kamonprasertsuk S, Suzuki S, Nanatani K, Oikawa H, et al. 2016. Significant heterogeneity and slow dynamics of the unfolded ubiquitin detected by the line confocal method of single-molecule fluorescence spectroscopy. *J. Phys. Chem. B* 120:8818–29
101. Phizicky EM, Fields S. 1995. Protein–protein interactions: methods for detection and analysis. *Microbiol. Rev.* 59:94–123
102. Song S, Xie T, Ravensbergen K, Hahm JI. 2016. Ascertaining effects of nanoscale polymeric interfaces on competitive protein adsorption at the individual protein level. *Nanoscale* 8:3496–509
103. Hirsh SL, McKenzie DR, Nosworthy NJ, Denman JA, Sezerman OU, Bilek MM. 2013. The Vroman effect: competitive protein exchange with dynamic multilayer protein aggregates. *Colloids Surf. B* 103:395–404
104. Vroman L, Adams A, Fischer G, Munoz P. 1980. Interaction of high molecular weight kininogen, factor XII, and fibrinogen in plasma at interfaces. *Blood* 55:156–59
105. Vroman L, Adams AL. 1969. Findings with the recording ellipsometer suggesting rapid exchange of specific plasma proteins at liquid/solid interfaces. *Surface Sci.* 16:438–46
106. Kisley L, Patil U, Dhamane S, Kourentzi K, Tauzin LJ, et al. 2017. Competitive multicomponent anion exchange adsorption of proteins at the single molecule level. *Analyst* 142:3127–31
107. Inoue G, Kawase M. 2016. Understanding formation mechanism of heterogeneous porous structure of catalyst layer in polymer electrolyte fuel cell. *Int. J. Hydrogen Energy* 41:21352–65

108. Craig AA, Imrie CT. 1999. Effect of backbone flexibility on the thermal properties of side-group liquid-crystal polymers. *Macromolecules* 32:6215–20
109. Bakry R, Bonn GK, Mair D, Svec F. 2007. Monolithic porous polymer layer for the separation of peptides and proteins using thin-layer chromatography coupled with MALDI-TOF-MS. *Anal. Chem.* 79:486–93
110. Cai Y, Chen Y, Hong X, Liu Z, Yuan W. 2013. Porous microsphere and its applications. *Int. J. Nanomedicine* 8:1111
111. Maaloum M, Pernodet N, Tinland B. 1998. Agarose gel structure using atomic force microscopy: gel concentration and ionic strength effects. *Electrophoresis* 19:1606–10
112. Gallagher S, Florea L, Fraser KJ, Diamond D. 2014. Swelling and shrinking properties of thermo-responsive polymeric ionic liquid hydrogels with embedded linear pNIPAAM. *Int. J. Mol. Sci.* 15:5337–49
113. Cooper JT, Peterson EM, Harris JM. 2013. Fluorescence imaging of single-molecule retention trajectories in reversed-phase chromatographic particles. *Anal. Chem.* 85:9363–70
114. Cooper J, Harris JM. 2014. Fluorescence-correlation spectroscopy study of molecular transport within reversed-phase chromatographic particles compared to planar model surfaces. *Anal. Chem.* 86:11766–72
115. Kisley L, Brunetti R, Tauzin LJ, Shuang B, Yi X, et al. 2015. Characterization of porous materials by fluorescence correlation spectroscopy super-resolution optical fluctuation imaging. *ACS Nano* 9:9158–66
116. Yamaguchi N, Zhang L, Chae B-S, Palla CS, Furst EM, Kiick KL. 2007. Growth factor mediated assembly of cell receptor-responsive hydrogels. *J. Am. Chem. Soc.* 129:3040–41
117. Dhar A, Samiotakis A, Ebbinghaus S, Nienhaus L, Homouz D, et al. 2010. Structure, function, and folding of phosphoglycerate kinase are strongly perturbed by macromolecular crowding. *PNAS* 107:17586–91
118. Langecker M, Arnaut V, Martin TG, List J, Renner S, et al. 2012. Synthetic lipid membrane channels formed by designed DNA nanostructures. *Science* 338:932–36
119. Dertinger T, Colyer R, Iyer G, Weiss S, Enderlein J. 2009. Fast, background-free, 3D super-resolution optical fluctuation imaging (SOFI). *PNAS* 106:22287–92
120. Hoyer P, de Medeiros G, Balázs B, Norlin N, Besir C, et al. 2016. Breaking the diffraction limit of light-sheet fluorescence microscopy by RESOLFT. *PNAS* 113:3442–6
121. Prabhat P, Ram S, Ward ES, Ober RJ. 2004. Simultaneous imaging of different focal planes in fluorescence microscopy for the study of cellular dynamics in three dimensions. *IEEE Trans. Nanobiosci.* 3:237–42
122. Ram S, Chao J, Prabhat P, Ward ES, Ober RJ. 2007. A novel approach to determining the three-dimensional location of microscopic objects with applications to 3D particle tracking. *Proc. SPIE 6443, Three-Dimensional and Multidimensional Microscopy: Image Acquisition and Processing XIV, San Jose, CA, Jan. 23–25*, 64430D. Bellingham, WA: SPIE
123. Huang B, Wang W, Bates M, Zhuang X. 2008. Three-dimensional super-resolution imaging by stochastic optical reconstruction microscopy. *Science* 319:810–13
124. Lien C-H, Lin C-Y, Chen S-J, Chien F-C. 2014. Dynamic particle tracking via temporal focusing multiphoton microscopy with astigmatism imaging. *Opt. Express* 22:27290–99
125. Power RM, Huisken J. 2017. A guide to light-sheet fluorescence microscopy for multiscale imaging. *Nat. Meth.* 14:360–73
126. Keller PJ, Schmidt AD, Wittbrodt J, Stelzer EHK. 2008. Reconstruction of Zebrafish early embryonic development by scanned light sheet microscopy. *Science* 322:1065–69
127. Badieirostami M, Lew MD, Thompson MA, Moerner WE. 2010. Three-dimensional localization precision of the double-helix point spread function versus astigmatism and biplane. *Appl. Phys. Lett.* 97:161103
128. Backer AS, Moerner WE. 2014. Extending single-molecule microscopy using optical Fourier processing. *J. Phys. Chem. B* 118:8313–29